Electrophysiology

After carrying out epifluorescent localization of GFP-labelled rI7 → M71 glomeruli in anaesthetized mice, we removed the bone over the olfactory bulb and targeted glass electrodes (2–10 MΩ, filled with 2 M sodium acetate) to rI7 → M71 glomerular regions. We made 10–15 electrode penetrations in each bulb to locate mitral cells associated with rI7 → M71. We isolated 137 cells from 15 mice at the characteristic mitral cell depth of 200–250 μm below the bulbar surface. All isolated cells were tested for response to octanal, heptanal and citral as described[10,13]. Data were digitally recorded at 30 kHz and analysed using Spike2 software (Cambridge Electronic Design Limited).

Tracer injections

Mice were anaesthetized (isoflurane, 1–3%) and the bone over the rI7 → M71 glomerular region was removed. An epifluorescence image was acquired to visualize the GFP-labelled rI7 → M71 glomerulus and its precise location was determined with respect to the surface map of blood vessels. Microinjections of rhodamine-labelled dextran, MW3000 (Molecular Probes) were targeted to either the rI7 → M71 glomerulus for tracing intrabulbar projections or to a region 150 μm beneath the glomerulus for tracing dendritic innervation. The tracer was iontophoresed (+2 μA, pulsed for 2–5 min) into the olfactory bulb through a micropipette. Mice were killed 8–12 h after injection for histological processing.

Histology and immunohistochemistry

Mice were anaesthetized 8–12 h after tracer injection (Nembutal, 100 mg/kg, i.p.) and perfused transcardially with PBS and 4% paraformaldehyde in 0.1 M phosphate buffer. Olfactory bulbs were removed, post-fixed (2 d) and cryoprotected (30% sucrose for 3 d). Bulbs were then sectioned on a freezing microtome at 40–50 μm, washed (PBS) and mounted (Vectashield, Vector Laboratories). To visualize the rI7 glomerulus, the rI7 → M71 YFP-G tissue was immunostained as floating sections with primary antibody against β-galactosidase (rabbit polyclonal, Cappel) at 1:1,000 dilution overnight at 4 °C. Cy3-conjugated secondary antibodies against goat (Jackson Immunoresearch) were used at 1:500 dilution for 2 h at 23 °C.

Confocal imaging

Sections were imaged on a Zeiss Axioskop 2 using a laser scanning confocal microscope (Zeiss LSM 510). Images were obtained with a 40 × (1.3 NA) oil objective for reconstructing individual glomeruli and 25 × (0.8 NA) oil objective for intrabulbar projections. YFP and GFP were excited with the 488-nm line of an argon laser and detected using a 522-nm emission filter. We acquired *z*-series projections using Zeiss LSM software.

Image analysis

We superimposed GFP images directly on intrinsic signal maps using IPLab (Scanalytics) to observe the colocalization of rI7 → M71 glomerulus with odorant activity. Signal intensity (I_s) measurements were determined by averaging a region of 5 × 5 pixels centred over the GFP peak pixel location for each experiment. Background values (I) were obtained at a distance of 50 pixels medial from the GFP peak. These values were used to calculate $\Delta I/I$ for each odorant. Intensity line profile measurements were obtained using NIH Image, and pixel values exported to Excel for graph-making and analysis. Measurements of glomerular size and intrabulbar projections were acquired using Zeiss LSM software and all statistical calculations were done in Excel.

Received 29 January; accepted 24 June 2002; doi:10.1038/nature01001.

1. Buck, L. & Axel, R. A novel multigene family may encode odorant receptors: a molecular basis for odor recognition. *Cell* **65,** 175–187 (1991).
2. Buck, L. B. The molecular architecture of odor and pheromone sensing in mammals. *Cell* **100,** 611–618 (2000).
3. Zhao, H. *et al.* Functional expression of a mammalian odorant receptor. *Science* **279,** 237–242 (1998).
4. Araneda, R. C., Kini, A. D. & Firestein, S. The molecular receptive range of an odorant receptor. *Nature Neurosci.* **3,** 1248–1255 (2000).
5. Bozza, T., Feinstein, P., Zheng, C. & Mombaerts, P. Odorant receptor expression defines functional units in the mouse olfactory system. *J. Neurosci.* **22,** 3033–3043 (2002).
6. Ressler, K. J., Sullivan, S. L. & Buck, L. B. Information coding in the olfactory system: evidence for a stereotyped and highly organized epitope map in the olfactory bulb. *Cell* **79,** 1245–1255 (1994).
7. Vassar, R. *et al.* Topographic organization of sensory projections to the olfactory bulb. *Cell* **79,** 981–991 (1994).
8. Mombaerts, P. *et al.* Visualizing an olfactory sensory map. *Cell* **87,** 675–686 (1996).
9. Wang, F., Nemes, A., Mendelsohn, M. & Axel, R. Odorant receptors govern the formation of a precise topographic map. *Cell* **93,** 47–60 (1998).
10. Rubin, B. D. & Katz, L. C. Optical imaging of odorant representations in the mammalian olfactory bulb. *Neuron* **23,** 499–511 (1999).
11. Johnson, B. A. & Leon, M. Modular representations of odorants in the glomerular layer of the rat olfactory bulb and the effects of stimulus concentration. *J. Comp. Neurol.* **422,** 496–509 (2000).
12. Uchida, N., Takahashi, Y. K., Tanifuji, M. & Mori, K. Odor maps in the mammalian olfactory bulb: domain organization and odorant structural features. *Nature Neurosci.* **3,** 1035–1043 (2000).
13. Belluscio, L. & Katz, L. C. Symmetry, stereotypy, and topography of odorant representations in mouse olfactory bulbs. *J. Neurosci.* **21,** 2113–2122 (2001).
14. Meister, M. & Bonhoeffer, T. Tuning and topography in an odor map on the rat olfactory bulb. *J. Neurosci.* **21,** 1351–1360 (2001).
15. Graziadei, P. P., Levine, R. R. & Graziadei, G. A. Regeneration of olfactory axons and synapse formation in the forebrain after bulbectomy in neonatal mice. *Proc. Natl Acad. Sci. USA* **75,** 5230–5234 (1978).
16. Bulfone, A. *et al.* An olfactory sensory map develops in the absence of normal projection neurons or GABAergic interneurons. *Neuron* **21,** 1273–1282 (1998).
17. Feng, G. *et al.* Imaging neuronal subsets in transgenic mice expressing multiple spectral variants of GFP. *Neuron* **28,** 41–51 (2000).
18. LaMantia, A. S. & Purves, D. Development of glomerular pattern visualized in the olfactory bulbs of living mice. *Nature* **341,** 646–649 (1989).
19. Buck, L. B. Information coding in the vertebrate olfactory system. *Annu. Rev. Neurosci.* **19,** 517–544 (1996).
20. Luo, M. & Katz, L. C. Response correlation maps of neurons in the mammalian olfactory bulb. *Neuron* **32,** 1165–1179 (2001).
21. Shipley, M. T. & Ennis, M. Functional organization of olfactory system. *J. Neurobiol.* **30,** 123–176 (1996).
22. Zou, Z., Horowitz, L. F., Montmayeur, J. P., Snapper, S. & Buck, L. B. Genetic tracing reveals a stereotyped sensory map in the olfactory cortex. *Nature* **414,** 173–179 (2001).
23. Schoenfeld, T. A., Marchand, J. E. & Macrides, F. Topographic organization of tufted cell axonal projections in the hamster main olfactory bulb: an intrabulbar associational system. *J. Comp. Neurol.* **235,** 503–518 (1985).
24. Liu, W. L. & Shipley, M. T. Intrabulbar associational system in the rat olfactory bulb comprises cholecystokinin-containing tufted cells that synapse onto the dendrites of GABAergic granule cells. *J. Comp. Neurol.* **346,** 541–558 (1994).
25. Buonviso, N., Chaput, M. A. & Scott, J. W. Mitral cell-to-glomerulus connectivity: an HRP study of the orientation of mitral cell apical dendrites. *J. Comp. Neurol.* **307,** 57–64 (1991).
26. Strotmann, J., Conzelmann, S., Beck, A., Feinstein, P., Breer, H. & Peter Mombaerts Local permutations in the glomerular array of the mouse olfactory bulb. *J. Neurosci.* **20,** 6927–6938 (2001).
27. Schaefer, M. L., Finger, T. E. & Restrepo, D. Variability of position of the P2 glomerulus within a map of the mouse olfactory bulb. *J. Comp. Neurol.* **436,** 351–362 (2001).
28. Katz, L. C. & Shatz, C. J. Synaptic activity and the construction of cortical circuits. *Science* **274,** 1133–1138 (1996).
29. Jefferis, G. S., Marin, E. C., Stocker, R. F. & Luo, L. Target neuron prespecification in the olfactory map of *Drosophila*. *Nature* **414,** 204–208 (2001).

Acknowledgements

We thank G. Feng for providing the YFP-G mice. L.C.K. is an Investigator in the Howard Hughes Medical Institute, L.B. is a Burroughs Wellcome Fellow in Neuroscience, and grant support to P.M. was from the NIH.

Competing interests statement

The authors declare that they have no competing financial interests.

Correspondence and requests for materials should be addressed to L.B. (e-mail: belluscl@ninds.nih.gov).

Prestin is required for electromotility of the outer hair cell and for the cochlear amplifier

M. Charles Liberman*†, Jiangang Gao†‡, David Z. Z. He§, Xudong Wu‡‖, Shuping Jia§ & Jian Zuo‡

* *Department of Otology and Laryngology, Harvard Medical School and Eaton-Peabody Laboratory, Massachusetts Eye & Ear Infirmary, Boston, Massachusetts 02114, USA*
‡ *Department of Developmental Neurobiology, St Jude Children's Research Hospital, Memphis, Tennessee 38105, USA*
§ *Boys Town National Research Hospital, Omaha, Nebraska 68131, USA*
‖ *Department of Anatomy and Neurobiology, University of Tennessee Health Science Center, Memphis, Tennessee 38163, USA*
† *These authors contributed equally to this work*

Hearing sensitivity in mammals is enhanced by more than 40 dB (that is, 100-fold) by mechanical amplification thought to be generated by one class of cochlear sensory cells, the outer hair cells[1–4]. In addition to the mechano-electrical transduction required for auditory sensation, mammalian outer hair cells also perform electromechanical transduction, whereby transmembrane voltage drives cellular length changes at audio frequencies *in vitro*[5–7]. This electromotility is thought to arise through voltage-gated conformational changes in a membrane protein[8,9], and prestin has been proposed as this molecular motor[10–12]. Here we show that targeted deletion of prestin in mice results in loss of outer hair cell electromotility *in vitro* and a

40–60 dB loss of cochlear sensitivity *in vivo*, without disruption of mechano-electrical transduction in outer hair cells. In heterozygotes, electromotility is halved and there is a twofold (about 6 dB) increase in cochlear thresholds. These results suggest that prestin is indeed the motor protein, that there is a simple and direct coupling between electromotility and cochlear amplification, and that there is no need to invoke additional active processes to explain cochlear sensitivity in the mammalian ear.

To test the hypotheses that prestin is the molecular motor underlying outer hair cell (OHC) electromotility and that OHC electromotility is the basis of the cochlear amplifier, we created a mutant mouse in which the *prestin* gene was targeted for deletion. Our targeting strategy (Fig. 1a) removed exons 3–7, which encode the 245 amino-terminal amino acids (about one-third of the protein). This strategy removed the ATG start codon, a highly conserved STAT motif, positively charged residues crucial for intracellular anion binding, and the first five of the twelve putative transmembrane domains[12]. Genomic Southern analysis (using both external and neomycin (Neo) probes) and polymerase chain reaction (PCR) analysis confirmed the targeted deletion of the *prestin* gene (Fig. 1b–d). Real-time PCR with reverse transcription (RT–PCR) analysis of the deleted coding region showed that the amount of prestin messenger RNA in heterozygous (+/−) cochleae was roughly half that in normal (+/+) cochleae, whereas no transcript was detected in cochleae from prestin null mice (−/−) (Fig. 1e). Immunohistochemistry with antibodies to the N- and carboxy-terminal segments of prestin[11] produced no signal in prestin null mice and reduced labelling in OHCs of heterozygous mice relative to that in wild-type mice (Fig. 2d–f; and data not shown).

The mutant mice had no obvious developmental or behavioural abnormalities, except for a small size difference: at 1 month, body weights of sex-matched prestin null ($n = 14$) and heterozygous ($n = 14$) mice were 85% and 95% of wild-type ($n = 16$) littermates,

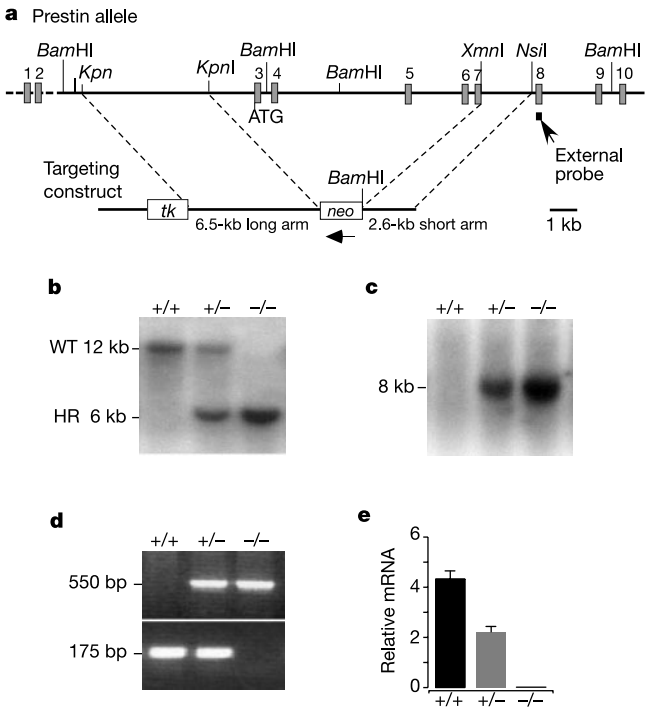

Figure 1 Targeted disruption of the prestin locus. **a**, Strategy for targeted deletion of the prestin gene. *tk*, thymidine kinase gene. **b**, Southern analysis of genomic DNA from wild-type (+/+), heterozygous (+/−) and prestin null (−/−) mice by using an external probe and *Bam*HI digestion. WT, wild type; HR, homologous recombination. **c**, Southern analysis with the Neo probe and *Bam*HI digestion. **d**, PCR genotyping of mutant mice. **e**, Real-time RT–PCR analysis of cochlear prestin mRNA in three genotypes, normalized to a standard sample. Means and standard errors shown (+/+, $n = 12$; +/−, $n = 9$; −/−, $n = 6$).

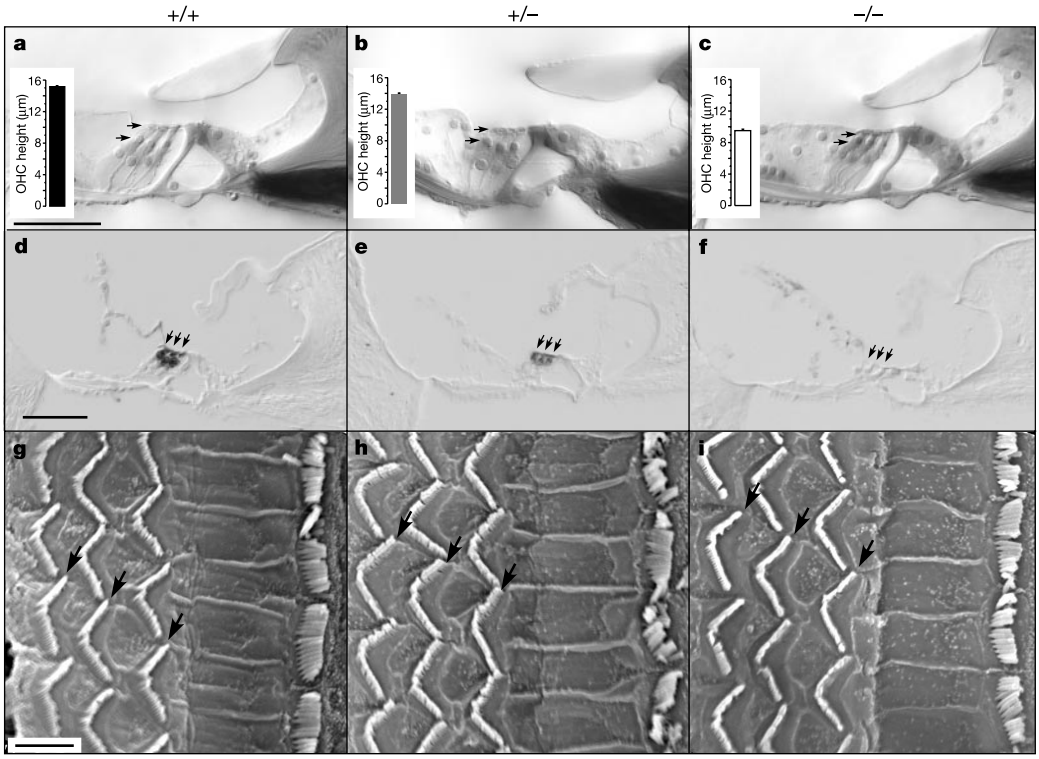

Figure 2 Morphological and immunohistochemical analysis of mutant mice. **a**–**c**, Light micrographs of the upper basal turn (cochlear frequency ~16 kHz) in cochleae of wild-type, heterozygous and null mice. Arrows at the cuticular plate and nucleus of third-row OHCs illustrate length differences in the three genotypes. Insets show mean lengths (±s.e.m.) of over 50 OHCs in the upper basal turn. Scale bar, 50 μm. **d**–**f**, Immunostaining for prestin N terminus shows three rows of darkly stained OHCs (arrows) in wild-type cochlea, less intense staining in heterozygous cochleae, and no prestin staining in ears of prestin null mice. Images are from the upper basal turn. Scale bar, 50 μm. **g**–**i**, Scanning electron micrographs show normal hair bundles on three rows of OHCs (arrows) from each of the three genotypes. Scale bar, 5 μm.

respectively. Cochlear morphology (Fig. 2a–c) in prestin null mice at 7–9 weeks of age was normal except for a decrement in OHC lengths in all cochlear turns (insets, Fig. 2a–c) and an almost complete loss of inner hair cells (IHCs) and OHCs in the basal 25% of the cochlear spiral (data not shown). The heterozygous mice had intermediate OHC lengths (inset, Fig. 2b) and showed scattered loss of IHCs and OHCs in the basal 25% of the cochlea. The finding of shortened OHCs is not surprising given that prestin is a principal component of the cell's lateral membranes[13]. The hair cell loss may reflect a developmental role for prestin in ion transport, as suggested by its homology to other transporters[14]—hair cell loss was not seen at post-natal day 7 (data not shown). Although prestin is expressed only in OHCs, IHC loss subsequent to primary OHC damage is well documented in the literature of acoustic injury[15].

Further morphological analysis suggested that the hair bundles, which house the machinery for mechano-electrical transduction, were normal in our mutant mice. Scanning electron micrographs showed normal hair bundle morphology on all rows of OHCs (Fig. 2g–i), and immunofluorescence showed that two principal components of the hair bundle machinery, myosin Ic and myosin VIIA[16,17], were present in OHCs of prestin null mice (data not shown).

To determine whether prestin is necessary for normal electromotility, OHCs were isolated from mice at 5–7 weeks of age. Normal mammalian OHCs show length changes *in vitro* when transmem-

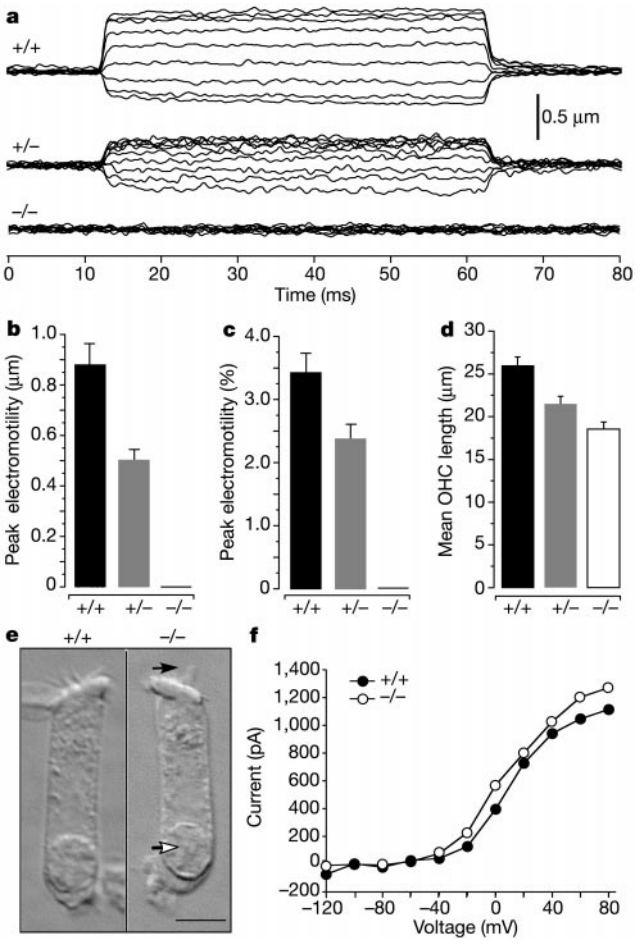

Figure 3 *In vitro* analysis of OHC electromotility in mutant mice. **a**, Length changes of OHCs of wild-type, heterozygous and null mice in response to voltage steps (−120–60 mV in 20-mV steps) in whole-cell, voltage-clamp recordings. Each trace is an average of five stimulus presentations. Cell contraction is plotted upward. **b**, Maximum motility measures for OHCs, expressed as absolute length change. **c**, Maximum motility for OHCs expressed as per cent length change. **d**, Lengths of isolated OHCs of each genotype. Sample sizes for **b**–**d**, 25 cells from +/+, 21 cells from +/− and 16 cells from −/−. Means and standard errors are shown. **e**, Micrographs of OHCs isolated from the apical turn of wild-type or null cochleae, with nucleus (open arrow) and stereocilia bundle (filled arrow) indicated. Scale bar, 5 μm. **f**, Current–voltage curves for representative OHCs from wild-type and null mice. The cells were held at −70 mV. *I–V* curves were obtained from measuring steady-state responses after the leak current was subtracted out using the *P/* − 4 technique. About 70% of series resistance was corrected. The uncompensated voltage error was less than 5 mV.

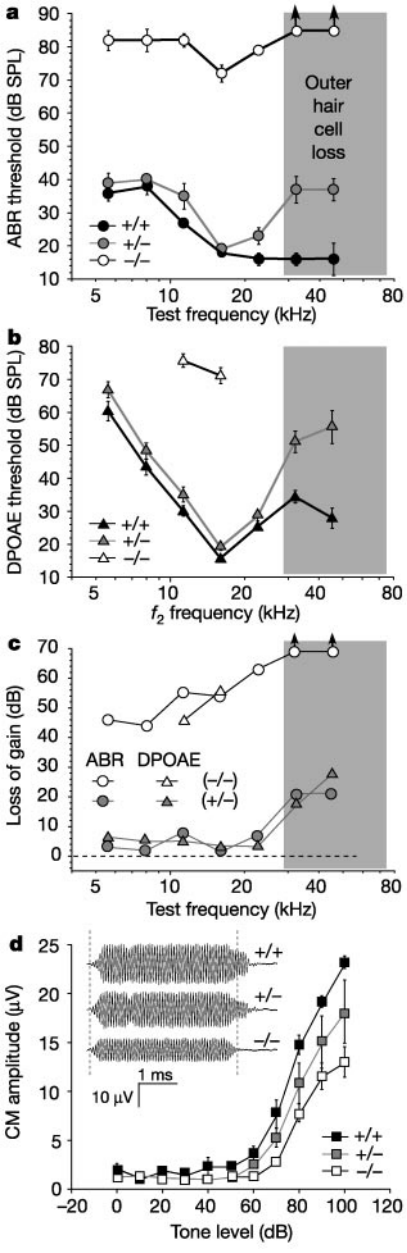

Figure 4 *In vivo* assays of cochlear sensitivity in mutant mice. **a**, Mean ABR thresholds (±s.e.m.) for five animals from each group. **b**, Mean DPOAE thresholds (±s.e.m.) for ten ears (both ears from five animals) from each group. For f_2 frequencies under 11.3 and over 16 kHz, DPOAE thresholds could not be measured in null mice, because passive system distortion produced a response at levels below the threshold for cochlear distortion. **c**, Contribution of prestin to cochlear amplification, as seen in threshold shifts of null and heterozygous relative to wild-type mice. Data are replotted from panels **a** and **b**. Grey areas in **a**–**c** correspond to the location where outer hair cell loss was observed in the cochlea of homozygous and heterozygous mice. **d**, Mean CM amplitudes (±s.e.m.) compared with sound pressure level for tone bursts at 16 kHz obtained from four animals of each genotype. Inset shows typical CM waveforms for each genotype in response to tones at 80 dB SPL. Dotted lines indicate onset and cessation of the tone burst.

brane voltage is changed under whole-cell voltage clamp (Fig. 3a, top). Outer hair cells isolated from prestin null mice at no point showed measurable motility ($n = 16$). The absolute magnitude of motility in heterozygous cells ($n = 21$) was roughly half that in wild-type cells ($n = 25$) (Fig. 3a–c). Consistent with the histological data (Fig. 2a–c), isolated OHCs also varied in length according to genotype (Fig. 3d, e). To assess whether the prestin deletion affected expression of ion channels, whole-cell currents were measured. No consistent difference was observed between wild-type and prestin null cells, as illustrated by current–voltage curves from OHCs of the apical turn of the cochlea (Fig. 3f).

To test whether prestin, and therefore OHC electromotility, is necessary for normal cochlear mechanical amplification, we obtained three measures of *in vivo* hair cell response from anaesthetized mice at 6–8 weeks of age.

The first measure, auditory brainstem response (ABR), represents synchronous electrical activity generated by neurons in the ascending auditory system and can be recorded from scalp electrodes by averaging responses to short tone bursts. By varying frequency, cochlear function can be assessed throughout the hearing range. In wild-type mice, ABR thresholds vary with frequency (Fig. 4a), from a sound pressure level (SPL) of 35 dB at 5.6 kHz (a relatively low frequency for a mouse) to 15 dB at 45.2 kHz (a relatively high frequency). In prestin null animals, ABR thresholds were 45–65 dB higher than those in wild-type mice, a decrease in sensitivity of two to three orders of magnitude (each 20 dB corresponds to a tenfold change in amplitude). In heterozygous animals, ABR thresholds for responses originating from cochlear regions with all hair cells present (frequencies $\leq$22.6 kHz) were elevated by 1–8 dB.

The second *in vivo* measure, distortion product otoacoustic emissions (DPOAEs), provides a more accurate measure of threshold elevations in heterozygous animals. DPOAEs are mechanical distortions created in the inner ear when two primary tones (f_1 and f_2) are presented. These distortions are amplified by OHCs, and propagated back through the middle ear to the ear canal, where they are measured in the sound pressure waveform. In prestin null mice, system distortion at high sound levels limited measurements to two test frequencies, however the threshold shifts in this region (45–55 dB) were similar to those seen with ABR. In heterozygous mice, DPOAE-based thresholds were 3.1–6.4 dB higher than those in wild-type mice, excluding the highest test frequencies (where OHC loss complicates interpretation). These small differences between the wild-type and heterozygous ears were statistically significant by a two-way analysis of variance (ANOVA; $P = 0.03$).

The final index of *in vivo* measure, the cochlear microphonic (CM), is an electrical response dominated by OHC receptor potentials[18]. CM can be recorded through a wire electrode on the surface of the cochlea, and it provides a measure of transducer function in OHCs. The CM amplitudes we observed (Fig. 4d) suggest that mechano-electrical transduction in mutant OHCs is intact. The CM reduction in the ears of heterozygous and prestin null mice is expected, given that CM is dominated by OHC potentials from the basal turn of the cochlea[18], and that as many as half of basal-turn OHCs are missing in the ears of prestin null mice. If OHC transducer currents were absent in the ears of null mice, the CM from remaining IHCs would be less than one-tenth the normal amplitude[18]. Note that CM waveforms from the ears of wild-type and heterozygous mice (Fig. 4d) show post-stimulus 'ringing', a cochlear 'echo' of the type expected in an 'active' ear[19]; however, in the ear of null mice, CM decays at the cessation of the tone burst, as expected for a passive system.

These results show that prestin is required for both OHC electromotility *in vitro* and normal cochlear amplification *in vivo*. In the absence of prestin, cochlear sensitivity is decreased in a frequency-dependent manner (Fig. 4c) from about 40 dB at 5.6 kHz to more than 60 dB at 22.6 kHz. The magnitudes of these shifts, and their frequency dependence, are consistent with estimates of cochlear amplifier gain as a function of cochlear frequency. These estimates are made on the basis of the physiologically labile, mechanical nonlinearities in basilar membrane motion[20–22], and, more indirectly, on frequency tuning curves of auditory nerve fibres[23]. Electromotility and cochlear sensitivity in the prestin heterozygous mouse also fit the simple view that *in vitro* motility and *in vivo* enhancement of cochlear sensitivity are directly coupled. The electromotility of heterozygous cells was roughly half (56%) that of normal cells (Fig. 3b), consistent with the idea that each prestin 'motor' makes an equal contribution to OHC length change and the assumption that heterozygous cells express half the number of prestin functional units. If these electrically induced length changes add linearly, *in vivo*, to the mechanical motion of the cochlear partition (at least near threshold values, where cochlear motion increases linearly with sound level[24]), then a halving of electromotility should be compensated for by a 6-dB increase in sound level. (In the logarithmic decibel scale, 6 dB corresponds to a factor of 2.) Correspondingly, the *in vivo* threshold elevation observed in ears of heterozygous mice was close to 6 dB (Fig. 4c).

The idea that OHC electromotility is the force generator for the cochlear amplifier has long been an attractive hypothesis; however, electromotility is absent in non-mammalian hair cells, which have threshold sensitivities rivalling the mammal[25]. Furthermore, active movement has been described in hair bundles, which may contribute to mechanical amplification in lower vertebrates[26,27]. The present data cannot rule out contributions from other cellular motors to the cochlear amplifier in the mouse. Nevertheless, our quantitative analyses of hair cell and cochlear function in prestin mutant mice suggest that no active process other than that provided by prestin-mediated electromotility need be invoked to explain the exquisite mechanical sensitivity of the mammalian cochlea. □

Methods

Generation of prestin mutant mice

Based on gerbil prestin complementary DNA sequence[10], we obtained three overlapping mouse prestin bacterial artificial chromosome (BAC) clones, 399N2, 427N18 and 577A16 (Research Genetics catalogue number 96050). The targeting construct using the NTK Scrambler vector (Stratagene) was transfected into 129/SvEv embryonic stem cells (AB2.2, Stratagene). Four out of 460 clones analysed underwent homologous recombination, identified by Southern blot analysis. The crosses between germline-transmitted heterozygous mice derived from one line yielded offspring with a 1:2:1 (51:105:52) ratio of the wild-type, heterozygous and null genotypes, and all F_2 mice used for further analysis are in a mixed background of 129/SvEv and C57B6/J. PCR primers for genotyping were from the deleted region (5′-GCTTGATGATTGGAGGTGTG-3′ and 5′-CTGAATGATT CCTGAAAGTAAGG-3′) and from the targeting vector (5′-CTGTTGTCCAAGTGCTT GCC-3′ and 5′-GATCGCTATCAGGACATAGCG-3′) (Fig. 1d).

Real-time quantitative PCR

We extracted total RNAs from post-natal day 9 (P9) cochleae and designed specific primers and probe for the N-terminal region: 5′–TCGGGCATAAGCACTGGG-3′, 5′-ACGGCTGCCAGCATGG-3′, TaqMan probe, 6FAM-TACTCCAGCTTCCCCAA GGCTTAGCCT-TAMRA. Prestin cDNA was made from a P14 wild-type testis and diluted to generate standard curves for every run of real-time PCR by using the ABI PRISM 7900 Sequence Detection System (Applied Biosystems) in 40 cycles. Cochlear homogenates from each animal were measured in triplicate. The relative quantities of prestin were calculated from standard curves and normalized to 18S (Applied Biosystems catalogue number 4310893E).

Histological analysis and immunocytochemistry

For plastic sections and scanning electron microscopy, mice were perfused with mixed aldehydes. For scanning electron microscopy, whole mounts of cochlear half turns were dried with hexamethyldisilazane, sputter-coated with platinum, and viewed with Philips ESEM XL30. For plastic sections, cochleae were osmicated, decalcified, dehydrated, embedded in plastic, and sectioned at 40 μm. Each cochlea was reconstructed in three dimensions, cochlear locations were computed and converted to frequency[28]. For immunohistochemistry, mice were perfused with 10% formalin or 4% paraformaldehyde, and cochleae were extracted, decalcified in EDTA, dehydrated, embedded in paraffin wax, and sectioned at 10 μm. Sections were incubated in primary antibody overnight followed by either biotinylated secondary antibodies or by fluorescently labelled secondary antibodies.

OHC motility assays

Outer hair cells were isolated from mouse cochleae as described for gerbil OHCs[29]. Cells were held at −70 mV, and 20-mV steps (−120–60 mV) were applied under whole-cell voltage-clamp. Recording pipettes had open-tip resistances of 3–5 MΩ and were filled with

internal solution containing 140 mM KCl, 2 mM $MgCl_2$, 10 mM EGTA, 10 mM HEPES at pH 7.2. The external solution was Leibovitz's L-15 (Gibco) containing 136 mM NaCl, 5.8 mM NaH_2PO_4, 5.4 mM KCl, 1.3 mM $CaCl_2$, 0.9 mM $MgCl_2$ at pH 7.2. Osmolarity was adjusted to 300 mosM l^{-1}. Motility was measured and calibrated using an electro-optical method in which the cell's ciliated pole was imaged through a rectangular slit onto a photodiode[29].

In vivo functional assays

For ABR, DPOAE and CM measurements, mice were anaesthetized with xylazine and ketamine. ABRs and DPOAEs were obtained from one set of animals; CMs from a second set. For ABR, needle electrodes were inserted at vertex and pinna. ABR and CM were evoked with 5-ms tone pips (0.5-ms rise–fall, with a $\cos^2$ envelope, at 35 per s). The response was amplified (× 10,000), filtered (0.1–3 kHz), and averaged with an A/D board in a PC-based data-acquisition system. Sound level was raised in 5-dB steps from 0 to 90 dB SPL. At each level, 1,024 responses were averaged (with stimulus polarity alternated) after 'artefact rejection'. Threshold was determined by visual inspection. For CM a silver-wire electrode was placed on the round window membrane. Responses to alternating pip polarities were subtracted, and the resultant waveform was digitally high-pass filtered to remove residual uncancelled neural potentials. The DPOAE at $2f_1 - f_2$ was recorded in response to two primary tones: f_1 and f_2, with $f_2/f_1 = 1.2$ and the f_2 level 10 dB lower than the f_1 level. Ear-canal sound pressure was amplified and digitally sampled at 4-μs intervals. Fast-Fourier transforms were computed from averaged waveforms of ear-canal sound pressure, and the DPOAE amplitude at $2f_1 - f_2$ and surrounding noise floor were extracted. Iso-response contours were interpolated from plots of amplitude versus sound level, performed in 5-dB steps of f_1 level. Threshold is defined as the f_1 level required to produce a DPOAE at 0 dB SPL.

Received 29 May; accepted 12 August 2002; doi:10.1038/nature01059.
Published online 28 August 2002.

1. Gold, T. Hearing. II. The physical basis of the action of the cochlea. *Proc. R. Soc. Lond. B* **135,** 492–498 (1948).
2. Dallos, P. & Harris, D. Properties of auditory nerve responses in absence of outer hair cells. *J. Neurophysiol.* **41,** 365–383 (1978).
3. Brown, M. C., Nuttall, A. L. & Masta, R. I. Intracellular recordings from cochlear inner hair cells: effects of stimulation of the crossed olivocochlear efferents. *Science* **222,** 69–72 (1983).
4. Dallos, P. The active cochlea. *J. Neurosci.* **12,** 4575–4585 (1992).
5. Brownell, W. E., Bader, C. R., Bertrand, D. & de Ribaupierre, Y. Evoked mechanical responses of isolated cochlear outer hair cells. *Science* **227,** 194–196 (1985).
6. Kachar, B., Brownell, W. E., Altschuler, R. & Fex, J. Electrokinetic shape changes of cochlear outer hair cells. *Nature* **322,** 365–368 (1986).
7. Ashmore, J. F. A fast motile response in guinea-pig outer hair cells: the cellular basis of the cochlear amplifier. *J. Physiol.* **388,** 323–347 (1987).
8. Ashmore, J. F. *Cochlear Mechanisms* (eds Wilson, J. P. & Kemp, D. T.) 107–116 (Plenum, London, 1989).
9. Santos-Sacchi, J. Reversible inhibition of voltage-dependent outer hair cell motility and capacitance. *J. Neurosci.* **11,** 3096–3110 (1991).
10. Zheng, J. *et al.* Prestin is the motor protein of cochlear outer hair cells. *Nature* **405,** 149–155 (2000).
11. Belyantseva, I. A., Adler, H. J., Curi, R., Frolenkov, G. I. & Kachar, B. Expression and localization of prestin and the sugar transporter GLUT-5 during development of electromotility in cochlear outer hair cells. *J. Neurosci.* **20,** RC116 (2000).
12. Oliver, D. *et al.* Intracellular anions as the voltage sensor of prestin, the outer hair cell motor protein. *Science* **292,** 2340–2343 (2001).
13. Forge, A. Structural features of the lateral walls in mammalian cochlear outer hair cells. *Cell Tissue Res.* **265,** 473–483 (1991).
14. Dallos, P. & Fakler, B. Prestin, a new type of motor protein. *Nature Rev. Mol. Cell Biol.* **3,** 104–111 (2002).
15. Bohne, B. A. & Rabbitt, K. D. Holes in the reticular lamina after noise exposure: implication for continuing damage in the organ of Corti. *Hear. Res.* **11,** 41–53 (1983).
16. Holt, J. R. *et al.* A chemical-genetic strategy implicates myosin-1c in adaptation by hair cells. *Cell* **108,** 371–381 (2002).
17. Kros, C. J. *et al.* Reduced climbing and increased slipping adaptation in cochlear hair cells of mice with Myo7a mutations. *Nature Neurosci.* **5,** 41–47 (2002).
18. Dallos, P. & Wang, C. Y. Bioelectric correlates of kanamycin intoxication. *Audiology* **13,** 277–289 (1974).
19. Kemp, D. T. Stimulated acoustic emissions from within the human auditory system. *J. Acoust. Soc. Am.* **64,** 1386–1391 (1978).
20. Johnstone, B. M., Patuzzi, R. & Yates, G. K. Basilar membrane measurements and the travelling wave. *Hear. Res.* **22,** 147–153 (1986).
21. Ruggero, M. A. & Rich, N. C. Application of a commercially-manufactured Doppler-shift laser velocimeter to the measurement of basilar-membrane vibration. *Hear. Res.* **51,** 215–230 (1991).
22. Sellick, P. M., Patuzzi, R. & Johnstone, B. M. Measurement of basilar membrane motion in the guinea pig using the Mossbauer technique. *J. Acoust. Soc. Am.* **72,** 131–141 (1982).
23. Kiang, N. Y. & Moxon, E. C. Tails of tuning curves of auditory-nerve fibers. *J. Acoust. Soc. Am.* **55,** 620–630 (1974).
24. Ruggero, M. A. Responses to sound of the basilar membrane of the mammalian cochlea. *Curr. Opin. Neurobiol.* **2,** 449–456 (1992).
25. Manley, G. A. Cochlear mechanisms from a phylogenetic viewpoint. *Proc. Natl Acad. Sci. USA* **97,** 11736–11743 (2000).
26. Fettiplace, R., Ricci, A. J. & Hackney, C. M. Clues to the cochlear amplifier from the turtle ear. *Trends Neurosci.* **24,** 169–175 (2001).
27. Hudspeth, A. J. Mechanical amplification of stimuli by hair cells. *Curr. Opin. Neurobiol.* **7,** 480–486 (1997).
28. Ehret, G. *The Auditory Psychobiology of the Mouse* (ed. Willott, J. F.)) 169–200 (Charles Thomas, Springfield, Illinois, 1983).
29. He, D. Z., Evans, B. N. & Dallos, P. First appearance and development of electromotility in neonatal gerbil outer hair cells. *Hear. Res.* **78,** 77–90 (1994).

Acknowledgements

We thank K. Cullen for technical assistance; T. Curran, B. Fritzsch, C. A. Shera and D. Freeman for comments on the manuscript; and B. Kachar, T. Hasson and P. Gillespie for antibodies. This work is supported in part by NIH grants to M.C.L., Z.Z.H. and J.Z., NIH Cancer Center Support CORE grant, and the American Lebanese Syrian Associated Charities (ALSAC).

Competing interests statement

The authors declare that they have no competing financial interests.

Correspondence and requests for materials should be addressed to J.Z. (e-mail: jian.zuo@stjude.org).

Robustness of the BMP morphogen gradient in *Drosophila* embryonic patterning

Avigdor Eldar*†, Ruslan Dorfman*, Daniel Weiss*†, Hilary Ashe‡, Ben-Zion Shilo* & Naama Barkai*†

** Department of Molecular Genetics and † Department of Physics of Complex Systems, Weizmann Institute of Science, Rehovot, Israel*
‡ School of Biological Sciences, University of Manchester, Manchester M13 9PT, UK

Developmental patterning relies on morphogen gradients, which generally involve feedback loops to buffer against perturbations caused by fluctuations in gene dosage and expression[1]. Although many gene components involved in such feedback loops have been identified, how they work together to generate a robust pattern remains unclear. Here we study the network of extracellular proteins that patterns the dorsal region of the *Drosophila* embryo by establishing a graded activation of the bone morphogenic protein (BMP) pathway. We find that the BMP activation gradient itself is robust to changes in gene dosage. Computational search for networks that support robustness shows that transport of the BMP class ligands (Scw and Dpp) into the dorsal midline by the BMP inhibitor Sog is the key event in this patterning process. The mechanism underlying robustness relies on the ability to store an excess of signalling molecules in a restricted spatial domain where Sog is largely absent. It requires extensive diffusion of the BMP–Sog complexes, coupled with restricted diffusion of the free ligands. We show experimentally that Dpp is widely diffusible in the presence of Sog but tightly localized in its absence, thus validating a central prediction of our theoretical study.

Graded activation of the BMP pathway subdivides the dorsal region of *Drosophila* embryos into several distinct domains of gene expression. This graded activation is determined by a well-characterized network of extracellular proteins[2,3], which may diffuse in the perivitelline fluid[4] that surrounds the embryo (Fig. 1a). The patterning network is composed of two BMP class ligands (Scw and Dpp), a BMP inhibitor (Sog), a protease that cleaves Sog (Tld) and an accessory protein (Tsg), all of which are highly conserved in evolution and are used also for patterning the dorso-ventral axis of vertebrate embryos[5]. Previous studies have suggested that patterning of the dorsal region is robust to changes in the concentrations of most of the crucial network components. For example, embryos that contain only one functional allele of *scw*, *sog*, *tld* or *tsg* are viable and do not show any apparent phenotype. Misexpression of *scw* or of *tsg* also renders the corresponding null mutants viable[6–8].

To check whether robustness is achieved at the initial activation gradient, we monitored signalling directly by using antibodies that recognize specifically an activated, phosphorylated intermediate of

